New Functionality Materials, Volume C
Synthetic Process and Control of Functionality Materials
T. Tsuruta, M. Doyama, M. Seno (editors)

Electronic structure and mechanism in surface-molecule interacting system

H. Nakatsuji

Department of Synthetic Chemistry, Faculty of Engineering, Kyoto University, Kyoto 606-01, Japan

Surface-molecule interactions and reactions are important elementary steps of catalytic reactions. Since they involve interactions between infinite and finite systems, modelling is necessary for theoretical investigations of catalytic reactions on a surface. The cluster model (CM) is most frequently used for quantum chemical calculations but neglects the effect of the bulk solid. For including such effect, (1) embedding the cluster onto a surface (actually into a larger cluster) is a method proposed by Grimley and Pisani, and (2) dipping the adcluster (admolecule + cluster) onto the electron bath of the solid and letting the system be at equilibrium for electron and spin exchanges is another model proposed by Nakatsuji. We show some applications of the CM, the embedding cluster model (ECM), and the dipped adcluster model (DAM). Roles of electron correlations and lower surface excited states, very important for surface chemistry, are investigated by the SAC-CI method proposed by our laboratory.

1. INTRODUCTION

Chemistry and physics of surface-molecule interaction and reaction systems are of much interest from both purely scientific and industrial standpoints. Since these interactions involve finite and infinite systems, modelling is necessary for theoretical investigations of these systems. Since the results of the investigations are largely dependent upon the nature and the quality of the model adopted, we have to carefully examine the models for surface-molecule interactions and reactions.

Electron correlations are very important since we are mostly interested in the system involving transition metals. Since surface has many dangling bonds, it usually has several lower excited states and further the catalytically active state is not necessarily the ground state, so that our theory should be able to deal with both ground and excited states in the same accuracy. Moreover, electron transfer is sometimes of crucial importance for surface electronic processes and therefore should be described accurately.

Cluster model (CM) has been most frequently used by quantum chemists for investigating chemisorptions and catalytic reactions on metal and semi-conductor surfaces. It also has a direct implication in the field of cluster chemistry growing up very rapidly in recent years. However, as a model of surface reactions, this model has a defect that it neglects the effect of bulk metal. For including such effect, Grimley, Pisani, and others proposed the embedded cluster model (ECM) [1-3] and Nakatsuji the dipped adcluster model (DAM) [4,5].

Here, we give a brief review on our recent *ab-initio* theoretical studies on surface-molecule interactions and reactions. In section 2, ECM is modified in order to be more easily applicable to *ab-initio* calculations, and it is applied to H_2 adsorption on a Li surface [6]. DAM is explained briefly in section 3, and the DAM studies on chemisorptions of O_2 on Ag [7-9] and Cl_2 on alkali metal [10] are shown in sections 4 and 5, respectively. CM is used for the studies of H_2 adsorption on a ZrO_2 semi-conductor surface [11], which is shown in section 6.

2. EMBEDDED CLUSTER MODEL

Cluster model is based on the locality of surface-molecule interactions and it is proved that the CM is useful for clarifying the mechanism of chemsorption and electronic structures of active sites. In the previous *ab-initio* calculations on small Li clusters, various adsorption sites were compared. The bridge or hole site of the Li (100) surface have been found to be most favorable, though the energy differences among the bridge, hole, and on-top sites were rather small. However, the CM does not include the effect of the bulk solid and suffers from an artificial boundary effect due to a finite size of the cluster. The calculated adsorption energy depends on the cluster

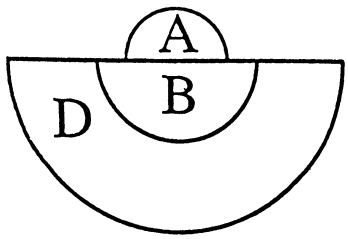

Fig. 1. Schematic representation of the embedded cluster model. A is the adsorbate, B the cluster, and D represents the solid.

size. The heats of atomic hydrogen adsorption on a Li cluster are reported to vary from 5 to 70 kcal/mol for different Li clusters.

Grimley and Pisani proposed earlier the method in which the surface-adsorbate system is embedded on a surface (actually on a larger cluster) and is attempted to connect with the outer surface region. In this work, we adopt the moderately large embedded cluster (MLEC) method of Ravenek and Geurts based on the Green's function method [1-3]. For *ab-initio* calculations, the size of the metal cluster appearing in the model is very important; it is difficult to use a moderately large cluster for representing the solid. We therefore modify the MLEC method such that the calculational labour is reduced by modifying the Green's function method and some other computational techniques and have coded an *ab-initio* program.

2.1. Theory

The surface-adsorbate system is illustrated in Fig. 1, where the adsorbate is represented by A and the solid surface by B ∪ D. In the CM, the system is represented by the cluster B interacting with the adsorbate A. In the ECM, the self-consistent-field (SCF) calculation on A ∪ B region is performed with considering the effect of D. The embedding scheme is performed based on the Hartree-Fock approximation. Let the interaction between A and D is small enough, and supposing that in the adsorption of A on B, the interaction between B and D is constant. We estimate the change of the electron density of A ∪ B by the effect of D and give an analytic form of the corrected density matrix by using the Green's function method. We adopt a large cluster as a B ∪ D, and give a line width to each discrete energy level of a cluster for simulating the density of states of a bulk metal by modifying the Green's function. This modification and the use of partially orthogonalized basis set improve the density of states of A ∪ B. Test calculations show that these modifications and new convergence algorithm make the SCF calculation possible.

2.2. Application to H_2 adsorption on a Li surface

The ECM has been applied to the adsorption of an H_2 molecule on a Li (100) surface. We use Li_{10} and Li_{14} cluster shown in Fig. 2 as the B ∪ D region. The shaded four atoms represent the B region

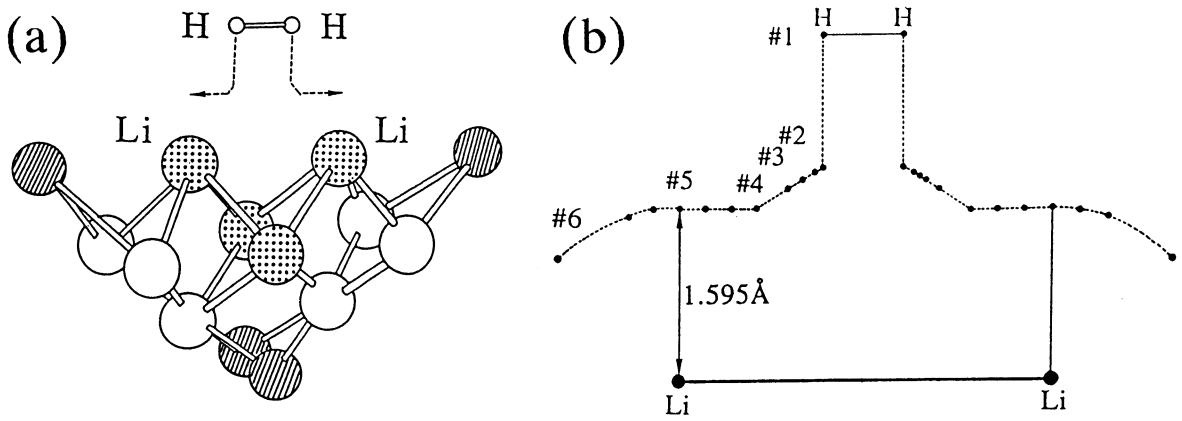

Fig. 2. (a) Li_n model cluster and (b) reaction pathway of H_2. Li_{10} and Li_{14} clusters interacting with H_2. The four shaded Li atoms compose the B region and the other Li atoms the D region and H_2 is the adsorbate A in Fig. 1. The four hatched atoms is excluded in the Li_{10} cluster.

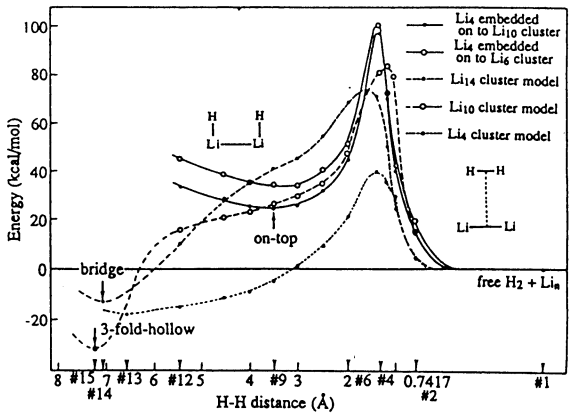

Fig. 3. Potential curves for the H_2 adsorption on a Li surface. The solid line represents the ECM, the broken and dotted line the CM. The most stable geometries for the CMs which are #13-#15 geometries are shown in Fig. 2.

and the others the D region. The clusters are supposed to represent the Li surface and to keep the bulk lattice structure throughout the hydrogen-adsorption processes. The H_2 molecule is assumed to approach horizontally, and interacts mainly with the shaded atoms.

We perform five different calculations for the cluster and embedded cluster calculations in order to clarify the embedding effect; they are Li_4 cluster, Li_4 embedded in Li_6 and Li_{10} giving Li_{10} and Li_{14} B∪D clusters, respectively, and Li_{10} and Li_{14} full-cluster models. These five calculations are performed on the same reaction path shown in Fig. 2.

The potential energy curves along the reaction path are shown in Fig. 3. The energy at point 1 is chosen as a standard, namely to be zero. The solid, broken and dotted lines represent the results of the ECM calculations, Li_{10} and Li_{14} CM calculations, and Li_4 CM calculations, respectively.

The value and the position of the energy barrier in the CM are strongly dependent on the cluster size, but in the embedded model they are less dependent on the size of the D region. The energy difference between the two ECMs are less than 10 kcal/mol all over the reaction path and their potential curves are similar. The ECMs give the sharp barrier of the height of 98~101 kcal/mol at point 5 and the local minimum corresponding to the on-top adsorption at point 9. The CMs do not give the minimum in the reaction path from point 1 to 12.

Figure 4 shows the equilibrium geometry of the H atoms and the gross charges on each hydrogen atom. In the Li_4 cluster, a single Li-H bond is formed with the terminal Li atom. The Li_{10} cluster adsorbs hydrogen atom at the three-fold-hollow site and each hydrogen atom makes equivalent three Li-H bonds with Li_3 on the corner. The Li_{14} cluster adsorbs the hydrogen atom at the bridge site and each hydrogen makes equivalent two Li-H bonds. These results on the adsorption site and the adsorption energy obtained for the CM are different from those obtained from the ECM; on top adsorption with negative adsorption energy (-34.9 or -24.7 kcal/mol) as shown in Fig. 4. The atomic charges of the adsorbed hydrogen decrease from -0.2 to -0.3 with embedding.

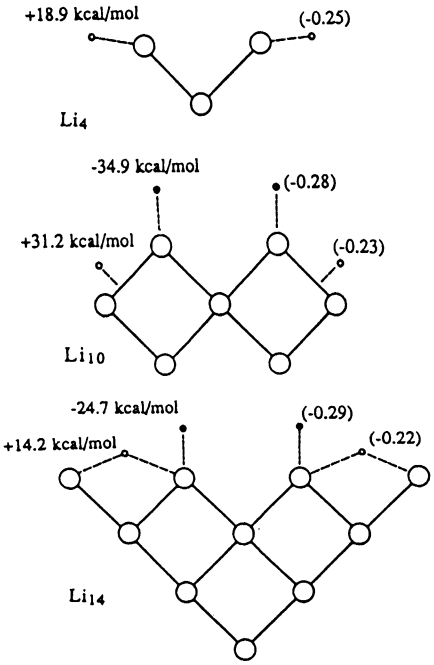

Fig. 4. Adsorption site, adsorption energy (relative to Li_n+H_2 in kcal/mol), and gross charge (in parentheses) of the adsorbed hydrogen. Filled and open small circles represent the results of the ECM and the CM, respectively.

2.3. Remarks

In summary, we have modified here the MLEC model and improved the convergence behavior of the MLEC method. The calculations of hydrogen adsorption on Li (100) surface are performed by the use of several CM and ECM. In the ECM, the equilibrium structure of the adsorbed hydrogen is obtained at the on-top position, but this adsorption structure is 24.7 or 34.9 kcal/mol less stable than

the isolated system. The CMs, on the other hand, show the three-fold-hollow or bridge site adsorption which are 14.2 and 31.2 kcal/mol more stable than the isolated system.

The criticism of the present result is rather difficult. If the results of the ECM should reproduce those of the full-cluster model, the results shown in Fig. 3 is by no means favorable to the ECM. On the other hand, if the D region of the ECM should be considered as representing a boundary of the bulk metal instead of an outer part of the larger cluster, the present result shown in Fig. 3 is difficult to evaluate since there are no experimental estimation on the potential surface for the dissociative adsorption of H_2 on a Li surface.

3. DIPPED ADCLUSTER MODEL (DAM)

For surface-molecule interacting systems in which electron transfer between surface and admolecule is important, the CM and the ECM are insufficient as far as the cluster size is not large enough. However, there are many cases in which electron transfer seems to be very important; oxygen and halogen chemisorptions on a metal surface, the roles of alkali metals and halogens as promoters, and the activity of electro-positive metals for dissociative adsorptions of CO, N_2, etc. The DAM [4,5] has been proposed for dealing with such systems. Since this model has been published five years ago, the accounts are given only briefly for being pertinent to the following applications.

Figure 5 illustrates the concept of the DAM. The adcluster is a combined system of an admolecule and a cluster and it is dipped onto the electron "bath" of the bulk metal. Then, electron and spin exchanges occur between the adcluster and the solid until the equilibrium is established for the exchange. The equilibrium condition is described with the use of the chemical potentials of the adcluster and the solid surface. Namely, at equilibrium, the adcluster is at the min[$E(n)$] in the range,

$$-\frac{\partial E(n)}{\partial n} \geq \mu \qquad (1)$$

where $E(n)$ is the energy of the adcluster with n being the number of electrons transferred from the bulk metal to the adcluster and μ the chemical potential of the electrons of the metal surface. We note that n may be a non-integer since we are dealing with a partial system. In this model, the cluster

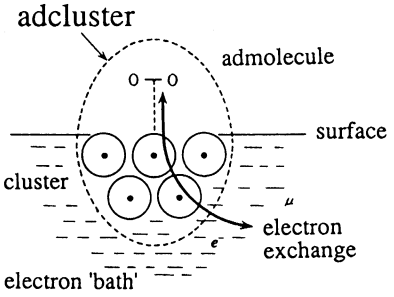

Fig. 5. Illustration of the concept of the dipped adcluster model.

atoms need not to supply all the electrons transferred into the adcluster: some are supplied from the electron bath of the solid.

Previously, we explained several general behaviors of the $E(n)$ curves and their implications. Depending on the shape of the $E(n)$ curve, either a partial electron transfer or one or two (integral) electron transfer may occur. We have proposed the molecular orbital model of the dipped adcluster. We have assumed that only the active MO of the adcluster, such as HOMO, LUMO, or SOMO, is partially filled in the electron-transfer process. There are two extreme ways of spin occupation in the active MO. One is the highest spin coupling in which α spin electron is first occupied and after the occupation reaches unity, the β spin electron is then added. The other is the paired spin coupling in which equal number of α and β spin electrons occupy the active MO. The former model is locally paramagnetic and the latter always diamagnetic. Energetically, the former is more stable than the latter.

When an electron is transferred from a surface to an admolecule, the electrostatic interaction between them would become important. For a metal surface, the so-called image force would occur and its inclusion was described in Ref. [5]. For a semiconductor surface, the interaction should be more localized and such treatment was described in Ref. [4].

4. CHEMISORPTION OF O_2 ON Ag SURFACE

An oxygen molecule chemisorbed on a silver surface shows several important catalytic reactions.

In particular, partial oxidation of ethylene is one of the most useful reactions in chemical industry. A lot of studies have been performed for clarifying the nature of the oxygen species adsorbed on a silver surface. Spectroscopic studies have revealed the existence of at least four adsorbed species; namely, physisorbed species (O_2), molecularly adsorbed species, superoxide (O_2^-) and peroxide (O_2^{2-}), and dissociatively adsorbed species (O^- and/or O^{2-}). On the theoretical side, some relevant papers have been published in recent years. However, some difficult problems still remain in the theoretical studies. One is to describe theoretically both molecular and dissociative adsorptions, and another is to calculate reliable adsorption energy. Since all of the previous theoretical studies have used the CM, we think that these difficulties are due to the neglect of the effects of the bulk metal in the CM calculations. In this study, we investigate the electronic processes and mechanisms of molecular and dissociative adsorptions of an O_2 molecule on a Ag surface. We use DAM instead of the CM, and include effectively the effects of a bulk metal such as a transfer of electrons of a bulk metal into an admolecule and an image force on a metal surface.

4.1. Side-on adsorption

We first take Ag_2O_2 as an adcluster and consider side-on bridge form interaction [7,9]. Before doing electron correlation calculations, we have applied the molecular orbital model of the dipped adcluster using the highest spin coupling model. The resultant *E(n)* curve has shown the occurrence of one electron transfer from the bulk Ag solid to the adcluster. We have therefore performed electron-correlation calculations for the Ag_2O_2 anion as the adcluster using the symmetry adapted cluster (SAC) and SAC-configuration interaction (SAC-CI) methods [12-14], which are applicable to the ground and excited states of both neutral and electron transferred states. We have included all the valence electrons, together with the d electrons of Ag, into electron correlation calculations.

Figure 6 is a display of the potential curves for the process of O_2 approach onto Ag_2 dipped onto the metal bulk. The broken lines are the results without the electron transfer (n=0) and the solid one with the electron transfer (n=1). Without the electron transfer, the potential curve, denoted by $^3B_2$ (n=0), is repulsive so that the chemisorption does not occur. Another broken line, denoted by $^3A_2$ (n=0),

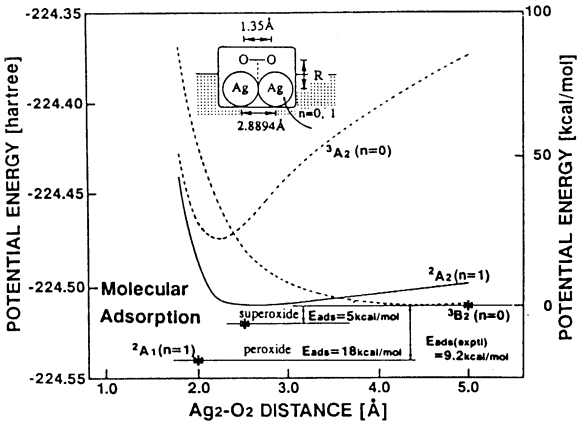

Fig. 6. Potential energy curves for the approach of O_2 onto Ag_2 in the Ag_2O_2 adcluster. *n* denotes the number of electrons transferred from the bulk metal to the adcluster.

corresponds to the electron transferred state within the adcluster from Ag_2 to O_2. Though this state is attractive, the minimum is less stable than the separated system which is $^3B_2$. Though these curves include the image force corrections, they essentially correspond to the CM calculations and do not explain the occurrence of the O_2 chemisorption. On the other hand, the potential given by the solid line, which is for the electron transferred state of the DAM, stabilizes as O_2 approaches Ag_2. The asterisk at about 2.5 Å is obtained by the optimization of the O-O distance and corresponds to the superoxide state. The calculated adsorption energy is 5.5 kcal/mol. Near 2.0 Å, there is another minimum corresponding to the peroxide state and the adsorption energy is 17.8 kcal/mol. The experimental molecular adsorption energy is 9.2 kcal/mol. Thus, the adsorption energy calculated by the DAM is positive and agrees well with the experimental value.

We next study the potential curve for the O-O stretching on a silver surface using again the Ag_2O_2 adcluster. Figure 7 shows the results. The lowest solid curve is for the peroxide and the upper two curves for the superoxide. As shown in the figure, the calculated vibrational frequencies agree quite well with the experimental values, showing that the molecular adsorption states expressed by the DAM correspond well to the actual systems observed experimentally. In Fig. 7, a point of disappointment at a first glance is a lack of the dissociatively adsorbed state. Up to the O-O distance of 2.8874 Å,

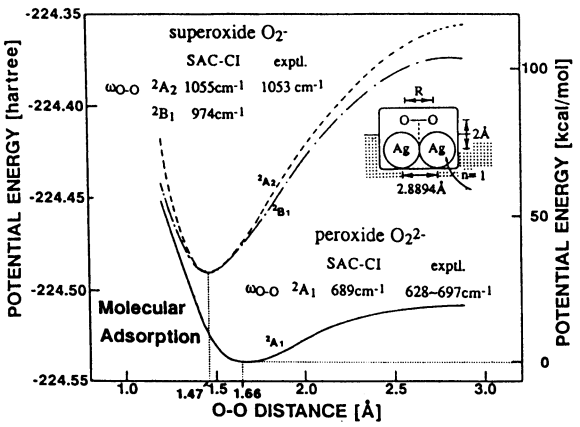

Fig. 7. Potential energy curves for the O-O elongation in the Ag_2O_2 adcluster.

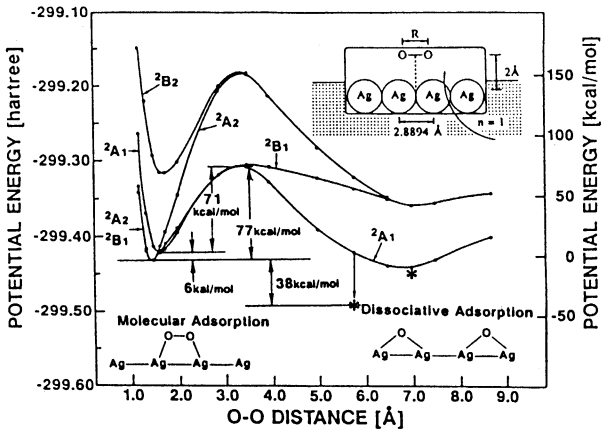

Fig. 8. Potential energy curves for the O-O dissociation in the Ag_4O_2 adcluster.

which is the distance of the Ag lattice, the potential monotonically increases. However, at this distance, we found that the gross charge on oxygen is -0.72, so that the electrostatic repulsion between the two oxygens amounts as large as 60 kcal/mol. Therefore, we expect that if we further elongate the O-O distance, we should get a stabilization which might lead to the second minimum corresponding to the dissociatively adsorbed state. For this purpose, we undertake the DAM calculation for O_2 on the linear Ag_4.

The results for the Ag_4-O_2 adcluster are displayed in Fig. 8. We certainly get two different potential minima. The minima at around 1.5-1.7 Å correspond to the molecular adsorption states (superoxide and peroxide) and another minimum at about 6-7 Å to the dissociatively adsorbed state. The dissociative state is obtained from the peroxide molecular adsorption state. After the optimization of the O-O and Ag-O distances, the dissociated state is calculated at the asterisk at the O-O distance of 5.78 Å. The dissociative state is calculated to be more stable than the molecular adsorption state by about 40 kcal/mol: the corresponding experimental value is 31-33 kcal/mol. Thus, using the DAM and the SAC-CI method, we could successfully describe the O_2 chemisorption on a Ag surface. The inclusions of the electron transfer from the bulk Ag metal to the adcluster and the electrostatic image force correction described by the DAM, and the electron correlations for several lower surface states described by the SAC-CI method are the reason of the success of the present study.

4.2. End-on adsorption

We have studied separatively on the end-on adsorption of O_2 on a Ag surface with the use of the DAM [8]. Electron transfer from the bulk metal to the AgO_2 adcluster is also important for the occurrence of this chemisorption. In the end-on geometry, superoxide species is the ground state, and there are no peroxide species in the lower energy region. The O-O axis of the superoxide is inclined by 70 ~ 80 degree from the surface normal. The outside oxygen atom of the adsorbed species seems to be more reactive than the inside one, while the net charge on the former is smaller than that on the latter. These results seem to show that the superoxide in the end-on form is favorable for the catalytic epoxidation of ethylene.

5. HALOGEN CHEMISORPTION ON AN ALKALI METAL SURFACE

Halogen chemisorption on an alkali metal surface involves interesting electron transfer processes from the surface to the halogen molecule. They are 'harpooning', surface chemiluminescence, and surface electron emission. When a halogen molecule approaches to some distance from the surface, an electron jumps into the molecule: this large distance electron transfer is called 'harpooning'. When the

molecule receives an electron, it becomes an anion so that the molecule is elongated and at the same time, it is attracted to the surface. When it collides with the surface, the surface chemiluminescence and electron emission occur. They are the electron transfer processes from the surface to the molecule accompanied with the emissions of a photon and an electron, respectively. Up to three electrons are thus transferred from the surface to the molecule.

We investigate these electron transfer processes by the DAM and the SAC/SAC-CI method. The *ab-initio* calculations are performed using the program HONDO7 [15] for the SCF calculations and SAC85 [16] for the SAC/SAC-CI calculations. The alkali metal distance is fixed to that observed for the crystals (Na: 3.7083 Å, K: 4.6185 Å, Rb: 4.95 Å) and the work functions are 2.75 eV for Na, 2.30 eV for K and 2.16 eV for Rb metal.

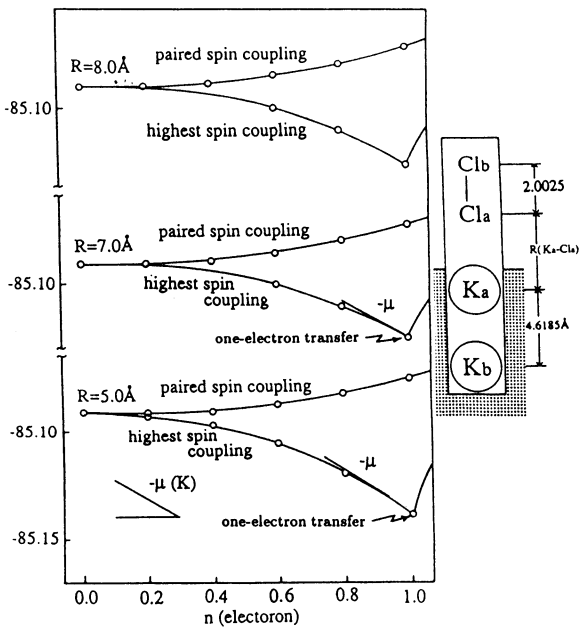

Fig. 9. *E(n)* curves calculated by the DAM for the Cl_2^- potassium surface system at the K_a-Cl_a distances of 8, 7, and 5 Å.

5.1. Harpooning

Harpooning is a long-distance jump of an electron from a metal surface to a molecule. It is explained as an electron tunnelling from the alkali metal surface to the halogen molecule. However, this process should be strongly vibronic, since the electron affinity of X_2^- is very much dependent on the X-X distance: a large electron affinity of X_2 is obtained only after an elongation of the distance.

We assume that Cl_2 molecule approaches the surface in the end-on form, since the σ^* MO of Cl_2 is the electron-accepting orbital. We think that the electron transfer occurs as a Franck-Condon process, so that the Cl-Cl distance is fixed to 2.0025 Å, theoretically optimized distance: the experimental equilibrium distance is 1.987 Å. We do not take into account molecular vibration effect. The alkali metal surface is represented by the two metal atoms dipped onto the electron bath of the alkali metal surface as illustrated in Fig. 9. We consider here only potassium surface.

We first apply the molecular orbital model for the DAM. The adcluster, K_2 interacting with Cl_2, is dipped onto the electron bath of the potassium metal whose chemical potential μ is 2.30 eV. Figure 9 shows the *E(n)* curves, calculated at different separations of Cl_2 from the surface. The curve is calculated by the paired spin coupling model and the highest spin coupling model and the active orbital is chosen to be the σ^* MO of Cl_2. In the paired spin coupling model, the energy of the system increases with increasing n, so that there is no place at which the tangent of the *E(n)* curve becomes equal to $-\mu$. However, in the highest spin coupling model, the *E(n)* curve is an upper convex and its tangent can become larger (in absolute value) than $-\mu$ when the Cl_a-K_a distance is smaller than 7 Å. Since the *E(n)* curve is an upper convex, this means that one electron (an integral number, one) is transferred from the surface to Cl_2. This one electron transfer is just the harpooning of an electron from the surface to Cl_2: this is the DAM picture of the harpooning. We note that we could explain the harpooning as a Franck-Condon process without resorting to the vibronic coupling. We also use the picture of 'tunneling' from the point on the *E(n)* curve at n=0 to the point at which the derivative $-E/n$ is equal to μ, since between these points the derivative is always less than μ. However, this concept of 'tunneling' on the n-space is different from that on the R-space.

Similar results were also obtained for the sodium-Cl_2 and rubidium-Cl_2 systems. In summary, the harpooning in the DAM picture is the Franck-Condon one-electron transfer process from the bulk alkali metal to Cl_2 in the highest-spin coupling mechanism. The harpooning distances calculated by the DAM are 6, 7, and 8 Å for Na, K, and Rb

surfaces, respectively. These distances are shorter than those estimated by the conventional tunneling mechanism: for example, it is estimated to be 10 Å for the Na surface.

5.2. Elongation and Chemisorption of Cl_2^-

The harpooning occurs at the Cl-Cl distance of 2.0025 Å, as a Franck-Condon process, and afterwards, the Cl-Cl distance is elongated with much stabilization of about 48 kcal/mol to the Cl-Cl distance of 2.64 Å. The binding energy of Cl_2^- on the surface is calculated to be only 7 kcal/mol: very weak even in comparison with the experimental binding energy, 29 kcal/mol of the free Cl_2^-. Since the energy gain by the elongation ~48 kcal/mol is much larger than the binding energy 7 kcal/mol, we expect that a neutral Cl atom is ejected out from the surface after the harpooning.

We assume that this excess energy is dissipated somewhere, say, to the alkali metal surface and calculate the adiabatic potential curve of Cl_2^- on the surface. The results show that starting from the K_a-Cl_a distance of 7 Å, the potential curve is attractive, and the minimum is obtained at the K_a-Cl_a distance of 3 Å. The stabilization energy there is about 27 kcal/mol.

5.3. Surface Chemiluminescence Process

We next study the surface chemiluminescence process: the second electron is transferred from the metal surface to the halogen molecule with an emission of a photon. We here take the reaction pathway of the adcluster K_2-Cl_2^- as shown in Fig. 10. The reaction is assumed to proceed from the end-on geometry on K_a, #1 and #2 positions, to the dissociated chemisorption structures, #8 and #9 positions. The Cl_a-K_a distance is 3.0 Å for #2 ~ #8, 3.25 Å for #1 and 2.5 Å for #9. The Cl_a-Cl_b distance at #1 and #2 is 2.73 Å.

An interesting question here invoked is "from where the second electron originates?". Does it originate from the bulk metal or from the local K_2 site directly interacting with Cl_2? In order to investigate this problem, we calculate by the SAC/SAC-CI method the total energies of the adclusters with the formal charges of K_2-Cl_2^{2-} and K_2^{2+}-Cl_2^{2-}, the former being the product of the electron transfer from the bulk metal and the latter from the local K_2 site. As a result, we find that the

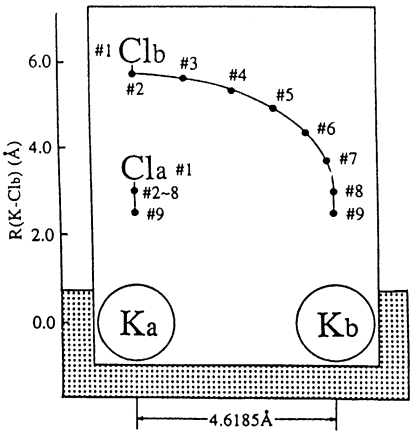

Fig. 10. Assumed reaction pathway for the surface chemiluminescence and electron emmision processes.

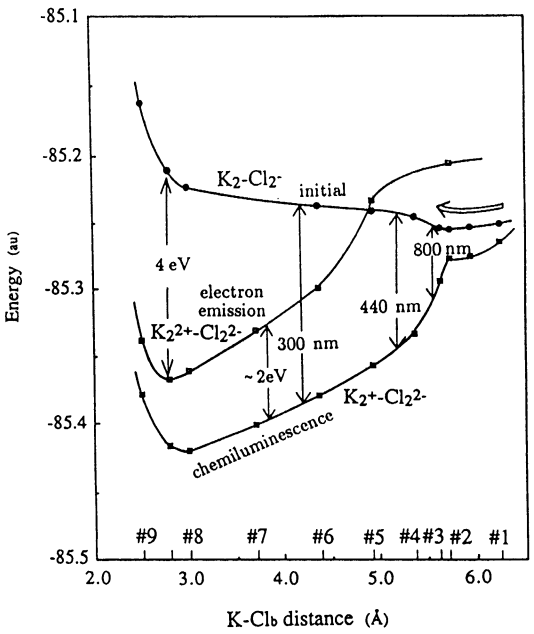

Fig. 11. Potential curves of the Cl_2-potassium surface system for the surface chemiluminescence and electron emmision processes calculated by the SAC/SAC-CI method.

latter is lower than the former for the geometries #2-#8. We therefore conclude that the second electron originates from the local K_2 site directly interacting with Cl_2^-.

We calculate the potential energy of the K_2-Cl_2^- adcluster (initial state) and the K_2^+-Cl_2^{2-} adcluster (final state) by the SAC-CI method. Figure 11 shows the result. The final state is denoted by 'chemiluminescence'. It also includes the final state of the electron emission discussed later. The system proceeds from the right to the left on the initial state curve, as shown by a big arrow, and makes a transition to the chemiluminescence final state with emitting a photon. The energy of the emitted photon is given by the energy difference of the initial and final states plus some part of the kinetic energy of the accelerated Cl_2^- in the initial state. The wave numbers shown in the figure correspond to the former one. Before #5 position, only the chemiluminescence transition occurs, but after there, two channels of transitions exist, namely, the chemiluminescence channel and the electron emission channel. Experimentally, the spectrum spreads from about 800 nm to 300 nm with the peak maximum at about 440 nm. The intensity rapidly decreases from about 400 nm to 300 nm. This rapid decrease is understood to be due to the transition to the electron emission channel: the crossing at about #5 geometry facilitates this transition. From Fig. 11 we see that the transition occurs at #3 ~ #6 geometries of the reaction path (Fig. 10): the transition occurs in the course of the dissociative chemisorption. The calculated transition probability has maximum at #3 geometry, while the experimental peak occurs between #4 and #5 geometries. This shift is probably due to an addition of the kinetic energy of Cl_2^- to the energy of the emitted photon.

The surface chemiluminescence process is certainly a charge transfer process from the surface to the halogen molecule. The gross charge at #4 geometry is Cl_b(-0.158), Cl_a(-0.778), K_a(-0.017), K_b(-0.047) in the initial state and Cl_b(-0.996), Cl_a(-0.947), K_a(+0.737), K_b(+0.206) in the final state.

5.4. Surface Electron Emission Process

We consider here the surface electron emission process. This is the two-electron process in which one electron is transferred from the surface to the halogen molecule anion X_2^-, and at the same time, another electron is emitted out of the surface. We assume that these two electrons belong to the local K_2 site directly interacting with X_2^-, since they are so strongly correlated in this process. It is difficult to expect such a strong correlation if one or two of these electrons belong to the electron bath of the bulk metal. We use the same reaction path as that used for the chemiluminescence process shown in Fig. 10.

Figure 11 also includes the potential curve for the final state of the surface electron emission calculated by the SAC-CI method. The initial state is common to both processes. The electron emission process occurs later to the chemiluminescence process, since the process proceeds from the right-hand side on the initial-state curve. The emission occurs in the geometries whose numbers are larger than #5, where the initial and final state curves of the electron emission cross to each other. The excess (kinetic) energy of the emitted electron is given by the energy difference between the initial and final states plus some part of the kinetic energy of the initial state. The former is about 4 eV at the turning point of the initial state curve, namely at about #8-#9 geometries, where the equilibrium geometry of the final state also exists: product KCl geometry. We therefore expect a large transition probability at #8-#9 geometries from these features of the potential curves of the initial and final states: the Franck-Condon factor should be large there. A large transition probability is also expected at the crossing point at about #5 geometry and may be calculated by the Landau-Zener model. Experimentally, the exoelectron energy distributions are measured for Cl_2 on yttrium and on Rb-dosed yttrium, and a maximum peak is seen at about 4 eV in accordance with the above expectation.

The final state of the electron emission process is almost the two potassium chloride. The charge distribution at #6 geometry is Cl_b(-0.936), Cl_a(-0.947), K_a(+0.956), and K_b(+0.927).

In Fig. 11, the difference between the final-state potential curves of the electron emission and the chemiluminescence is roughly about 2 eV at any geometry of the reaction pathway. This is because the difference corresponds to the work function of the potassium surface: the experimental value is 2.3 eV.

6. CHEMISORPTION OF H_2 ON ZrO_2 SURFACE

In recent years, spectroscopic investigations on the species chemisorbed on metal and metal oxide surfaces are actively performed. For example, on

ZnO and ZrO_2, metal-H and O-H stretching frequencies are clearly observed and their behaviors are well examined by IR spectroscopy [19-21].

We have studied the electronic mechanism for the dissociation of a hydrogen molecule over ZnO by using *ab-initio* MO calculations with Madelung potentials [22]. We found that the electrostatic field on the ZnO surface, represented as Zn^+ and O^-, works to polarize the σ and σ^* orbitals of H_2, and makes the interaction between H_2 and ZnO more favorable. We also investigated on the low lying excited states along the reaction path, and found that the excited states are not important for the dissociation of H_2.

On ZrO_2 surface, three types of H-H stretching and two types of Zr-H stretching were observed by IR spectroscopy [19]. This led to the suggestion that the three types of molecularly adsorbed sites exist on ZrO_2 surface, and that two types of dissociative adsorption exist: homolytic dissociation type and heterolytic dissociation type. In this report, the adsorption of a hydrogen molecule on a ZrO_2 surface is investigate by using CM in the Madelung potential. We study the geometries of molecular and dissociated adsorptions of H_2 on the ZrO_2 surface. We also investigate the reaction path for the dissociation of H_2 and the electronic mechanism for the reaction.

A Zr_3O_8 cluster is used as a model for the ZrO_2 surface. In this cluster, the central Zr-O pair is fully surrounded with the other Zr and O atoms. Hydrogen atoms are added to the terminal Zr and O in order to fill up their valencies. This cluster is shown in Fig. 12. A hydrogen molecule, as a reactant, is put above the central Zr-O. We carried out *ab-initio* RHF-SCF calculations for this H_2-$Zr_3O_8(H_8)$ system. The Madelung potential is used; +1 and -1 charges are put as shown in Fig. 12.

Molecularly adsorbed structures are shown in Fig. 13 (a,b). We found two types of hydrogen molecule on the cluster: one is a side-on structure on Zr (a) and the other is an end-on structure on O (b). Optimized geometrical parameters are also shown in Fig. 13. The third type of the molecularly adsorbed H_2 suggested by experiments could not be found within our trials. The structure of dissociative adsorption is shown in Fig. 13 (c). This structure is the heterolytic dissociation type, in which the Zr-H and O-H bonds are formed. The homolytic type, in which two hydrogen atoms are on a Zr atom, could not be found in our present investigation, so the existence of this species is somewhat obscure.

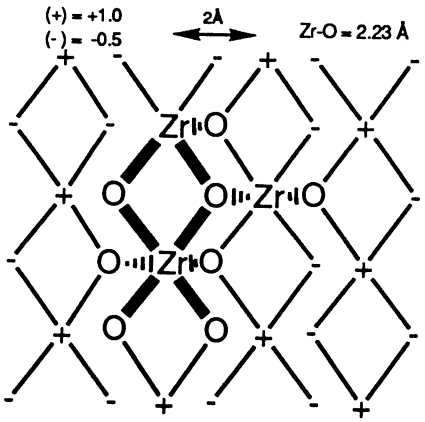

Fig. 12. Cluster model for ZrO_2 surface with Madelung potential ($Zr_3O_8H_8$).

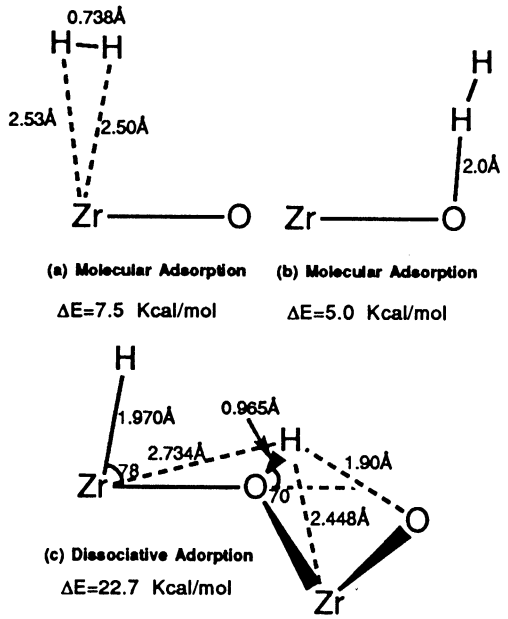

Fig. 13. Stable structures of hydrogen molecule and atom.

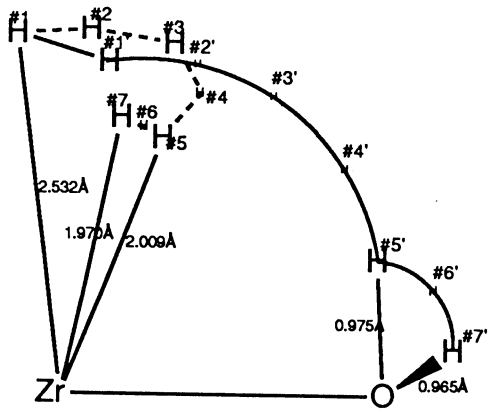

Fig. 14. Reaction path for the dissociation of a hydrogen molecule.

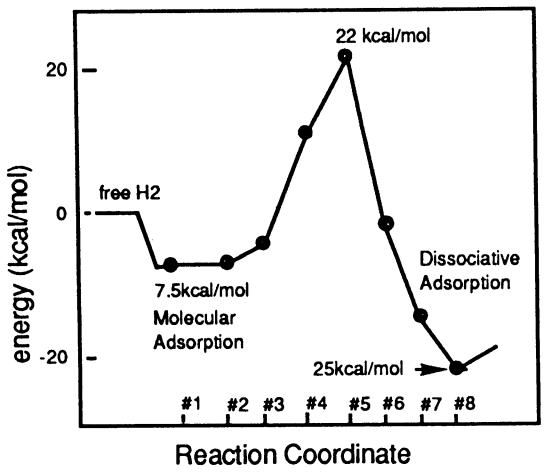

Fig. 15. Potential energy curve along the reaction path given in Fig. 14.

Next, we calculated the reaction path and the activation energy for the dissociative adsorption of a hydrogen molecule. The precursor of the reaction is assumed to be the molecularly adsorbed H_2 in Fig. 13 (a). The reaction path is shown in Fig. 14 and the total energy curve are in Fig. 15. At the first stage of the reaction, the H_2 molecule makes a circle around the Zr atom (#1-#3) toward the oxygen atom. At the point #1-#3, the change of the total energy is within a few kcal/mol, so this migration of H_2 is almost free. From #4 the internuclear distance of H_2 is gradually enlarged, the H atom of the right side moves to the O atom and the other H returns again to the Zr atom. The transition state exists at around #5 and the activation energy is 29.5 kcal/mol. This value could become smaller as we refine the reaction path.

The Zr atom on the surface has a vacant $5p_z$ orbital at low energy level and O atom has an occupied $2\sigma p_z$ orbital. The σ orbital of H_2 in Fig. 13 (a) is almost the same as that of a free H_2, so a small electron donation occurs from 5p(Zr) to $\sigma(H_2)$. When H_2 moves to the direction for the oxygen atom (#1-#3), σ and σ^* orbitals of H_2 are strongly polarized by the electronic field from the surface. This polarization of H_2 orbitals facilitates both 5p(Zr)-$\sigma(H_2)$ and 2p(O)-$\sigma^*(H_2)$ interactions, and causes the driving force of the reaction. At #6 the gross charges of the H atoms on the Zr side and the O side are -0.35 and +0.37, respectively.

7. CONCLUSION

We have investigated various types of surface-molecule interactions by the methodology of our laboratory: the dipped adcluster model and the SAC/SAC-CI method. It is shown that this methodology is powerful for investigating surface-molecule interactions and reactions occurring on metal and semiconductor surfaces, and in both thermal and photochemical situations. Based on this success, we are currently expanding the field of applications of our methodology, including surface photochemistry.

REFERENCES

[1] T. B. Grimley and C. Pisani, J. Phys. C7 (1974) 2831.
[2] C. Pisani, Phys. Rev. B17 (1978) 3143.
[3] W. Ravenek and F. M. M. Geurts, J. Chem. Phys., 84 (1986) 1613.
[4] H. Nakatsuji, J. Chem. Phys., 87 (1987) 4995.
[5] H. Nakatsuji, H. Nakai, and Y. Fukunishi, J. Chem. Phys., 95 (1991) 640.
[6] Y. Fukunishi and H. Nakatsuji, J. Chem. Phys.,

97 (1992) 6535.
[7] H. Nakatsuji and H. Nakai, Chem. Phys. Lett. 174 (1990) 283.
[8] H. Nakatsuji and H. Nakai, Can. J. Chem. 70 (1992) 404.
[9] H. Nakatsuji and H. Nakai, J. Chem. Phys. in press (1993).
[10] H. Nakatsuji, R. Kuwano, H. Morita, and H. Nakai, proceeding of the IVth International Symposium - Theoretical Approach to Catalysis at Interfaces, Cracow, Poland, July 27-31, 1992, to appear in Journal of Molecular Catalysis.
[11] M. Hada, H. Nakatsuji, K. Nagata, H. Ogawa, and K. Domen, submitted.
[12] H. Nakatsuji and K. Hirao, J. Chem. Phys. 68 (1978) 2035.
[13] H. Nakatsuji, Chem. Phys. Lett. 59 (1978) 362; 67 (1979) 329, 334.
[14] H. Nakatsuji, Acta Chimica Hungarica, in press (1992).
[15] J. K. Norskov, D. M. Newns, and B. J. Lundqvist, Surf. Sci., 80 (1979) 179.
[16] P. A. Dowben, CRC Crit. Rev. Solid State Mat. Sci., 13 (1987) 191.
[17] M. Dupuis, J. D. Watts, H. O, Viller, and G. J. B. Hurst, Program System HONDO7, Program Library No.544, Computer Center of the Institute for Molecular Science (1989).
[18] H. Nakatsuji, Program system for SAC and SAC-CI calculations, Program Library No. 146(Y4/SAC), Data Processing Center of Kyoto University, 1985; H. Nakatsuji, Program Library SAC85 (No. 1396), Computer Center of the Institute for Molecular Science, Okazaki, 1986.
[19] J. Lamotte and J. C. Lavalley, J. Chem. Soc. Faraday Trans., I81 (1985) 215.
[20] J. Kondo, K. Domen, K. Maruya, and T. Onishi, J. Chem. Soc. Faraday Trans., 86 (1990) 397.
[21] J. Kondo, K. Domen, K. Maruya, and T. Onishi, Chem. Phys. Letters, 188 (1992) 443.
[22] K. Fukunishi and H. Nakatsuji, Intern. J. Quantum Chem., 42 (1992) 1101.